J. Phys. D: Appl. Phys. **42** (2009) 055303 (7pp) doi:10.1088/0022-3727/42/5/055303

Aerosol palladium activation for electroless copper deposition and heat treatment with NO injection to fabricate Cu oxide/carbon fibre

Jeong Hoon Byeon[1], **Ryang Hwa Lee**[2] **and Jungho Hwang**[2,3,4]

[1] Digital Printing Division, Samsung Electronics Co., Ltd, Suwon 443-742, Republic of Korea
[2] Yonsei Center for Clean Technology, Yonsei University, Seoul 120-749, Republic of Korea
[3] School of Mechanical Engineering, Yonsei University, Seoul 120-749, Republic of Korea

Received 7 October 2008, in final form 18 November 2008
Published 17 February 2009
Online at stacks.iop.org/JPhysD/42/055303

Abstract
This paper introduces a novel method for fabricating copper (Cu) oxide/activated carbon fibre (ACF) through the aerosol palladium (Pd) activation for use in electroless Cu deposition and heat treatment of Cu deposited ACF with nitric monoxide (NO) gas injection. Electroless Cu deposition was initiated by catalytically activating the ACF surface with spark generated Pd aerosol nanoparticles. The catalytically activated ACF was placed into a solution used for the electroless Cu deposition. Subjecting the Cu deposited ACF to a heat treatment in a NO/nitrogen (N_2) gas injection (1000 ppm NO) resulted in changes to the morphology of the Cu particles. As the temperature increased from 100 to 500 °C, the relative mass fraction of oxygen in the Cu particles increased from 3.6% to 14.2% and the fraction of Cu decreased from 41.2% to 34.1%, which was caused by the formation of Cu oxides (Cu_2O and CuO). The corresponding surface area and pore volume of the ACF decreased from 1019 $m^2\,g^{-1}$ to 401 $m^2\,g^{-1}$ and from 0.40 $cm^3\,g^{-1}$ to 0.18 $cm^3\,g^{-1}$, respectively. The morphological evolution and decrease in porosity were attributed to volume expansion of Cu particles during oxidation.

1. Introduction

Fine metal oxide particles are of considerable interest because they can have physical and chemical properties that are characteristic of neither the atom nor the bulk. Oxides of transition metals, such as iron, nickel, cobalt, zinc and copper, have many important applications [1]. Copper oxides have been widely used in many areas such as in heterogeneous catalysts, anode electrodes for batteries, magnetic storage media and high temperature superconductors [2]. There have been many studies on the materials comprising the copper oxides and supports with the major focus being on the various interactions between the different phases as well as their applications, such as environmental, wear, material synthetic, energy and biological applications. Various copper oxide/support materials have been reported recently, such as composites [3, 4], catalysts [5–8], electrodes [9, 10], semiconductors [11, 12], reinforcements [13] or antimicrobial agents [14].

Activated carbon fibre (ACF) is highly microporous carbon material [15–17] that is commercially available in the form of fibre tows, cloths (fabrics), papers, mats and felts [18]. ACF is widely used in various separation, purification and catalytic processes [19]. Recently, ACF was used in electric-double-layer capacitors (EDLC) electrodes on account of its large specific surface area and high electrical conductivity [20–22].

According to fascinating properties of copper oxide, copper oxide/support and ACF, it seems very useful to fabricate copper oxide supported ACF and relating approach is seldom reported [23] in the literature for growing copper oxides on fibrous carbon substrate. In this study, we propose a novel process comprising an electroless copper deposition of ACF and a subsequent heat treatment of copper deposited ACF.

[4] Author to whom any correspondence should be addressed.

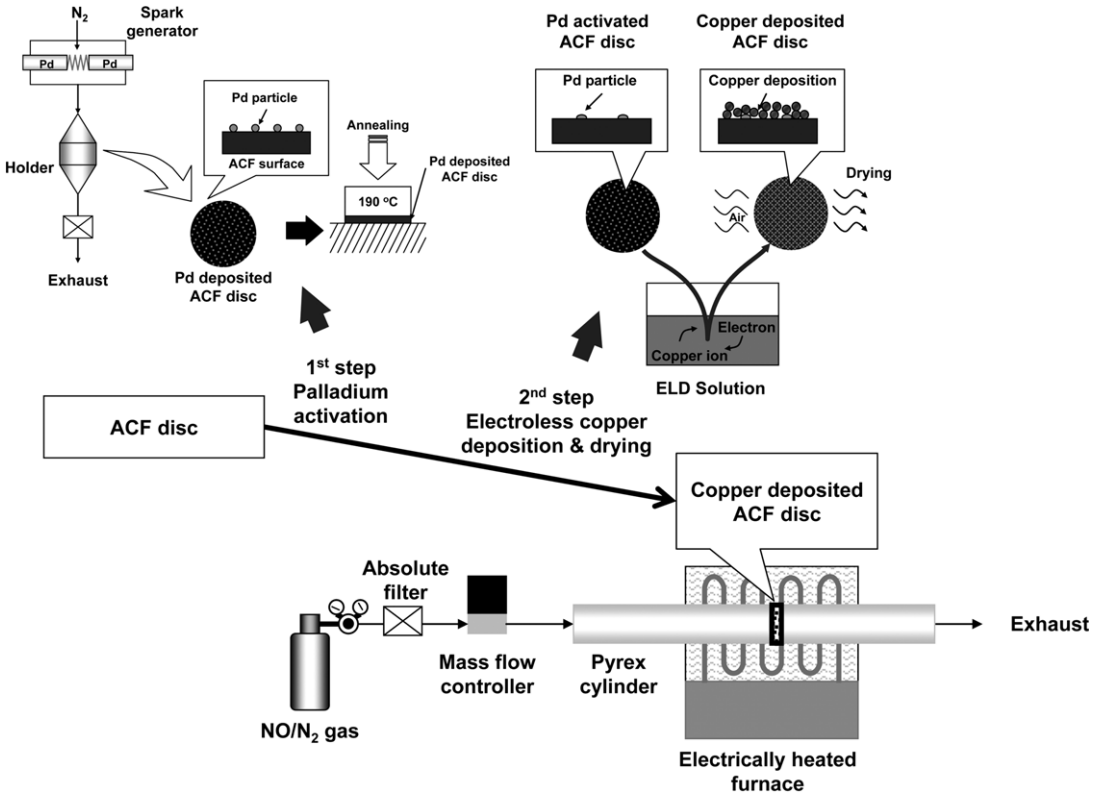

Figure 1. Overview of fabrication procedure.

The electroless deposition (ELD) technique enables metallic components to be deposited easily and uniformly in some channels of supports with a complex configuration such as fibre and particle, provided the deposition solution is in contact with the channel walls [24, 25]. The initiation of the ELD process is preceded by a surface activation to provide catalytic sites on the material surface [26, 27]. However, conventional activations (mainly tin–palladium based) require a long process time and intermittent water rinsing and drying, involve the loss of expensive metal ions and create environmental pollution problems [28]. Moreover, it seems very difficult to grow copper oxides on ACF from pure copper particles just by heat treatment as mentioned in [2] because of ACF burn-off at oxygen existed with high temperature.

In this paper, we present improved processes to overcome difficulties in using conventional catalytic surface activation and heat treatment. Since it is difficult to realize pure catalytic sites with a wet chemical activation method due to impurities inevitably involved, an aerosol activation using spark generated palladium nanoparticles is used to form catalytic sites on ACF surface. In addition, deposited copper particles on ACF surface are oxidized by a nitric monoxide (NO; N_2 balanced) gas injection at high temperature without any risk of burn-off or cracks of ACF, since it is known that thermal oxidation in an oxygen environment may cause burn-off or cracks of carbonaceous material and thus the fabrication of copper oxide/ACF structure is difficult. Previous studies [24, 29] have reported that copper particles were oxidized by a NO/inert gas flow at high temperatures without the need for additional oxygen injection, and nevertheless, details for formation of copper oxides were not described. Morphology and chemistry of aerosol palladium activated and copper deposited ACFs were determined using field emission scanning electron microscopy-energy dispersive x-ray spectroscopy (FESEM-EDX). Morphological and chemical evolution of the copper deposited ACF after the heat treatment were also observed by FESEM-EDX. X-ray diffraction (XRD) was used to identify the phases of copper deposited and the thermally treated ACF. The textural properties (surface area, pore volume and pore diameter) of the ACF were analysed by porosimetry.

2. Experimental

Figure 1 shows a schematic of the experimental setup. The catalytic surface activation involved the spark generation [30] of aerosol palladium nanoparticles and their fibrous filtration by rayon-based ACF (38 mm in diameter and 2.6 mm in thickness, KF-1600, Toyobo). A spark was generated between two identical palladium rods (diameter: 3 mm, length: 100 mm, Nilaco, Japan) inside a reactor under a pure nitrogen environment at STP [31–33]. The flow rate of the nitrogen gas, which was controlled by a mass flow controller, was set to 3 L min^{-1}. The electrical circuit specifications were as follows: resistance of 0.5 MΩ, capacitance of 10 nF, loading current of 2 mA, applied voltage of 3 kV and frequency of 667 Hz. In order to prevent the detachment of the nanoparticles from the surface of the ACF, the ACF was separated from the holder and annealed in air at 190 °C for 5 min. Once the ACF was activated by the aerosol process, the ACF was immersed

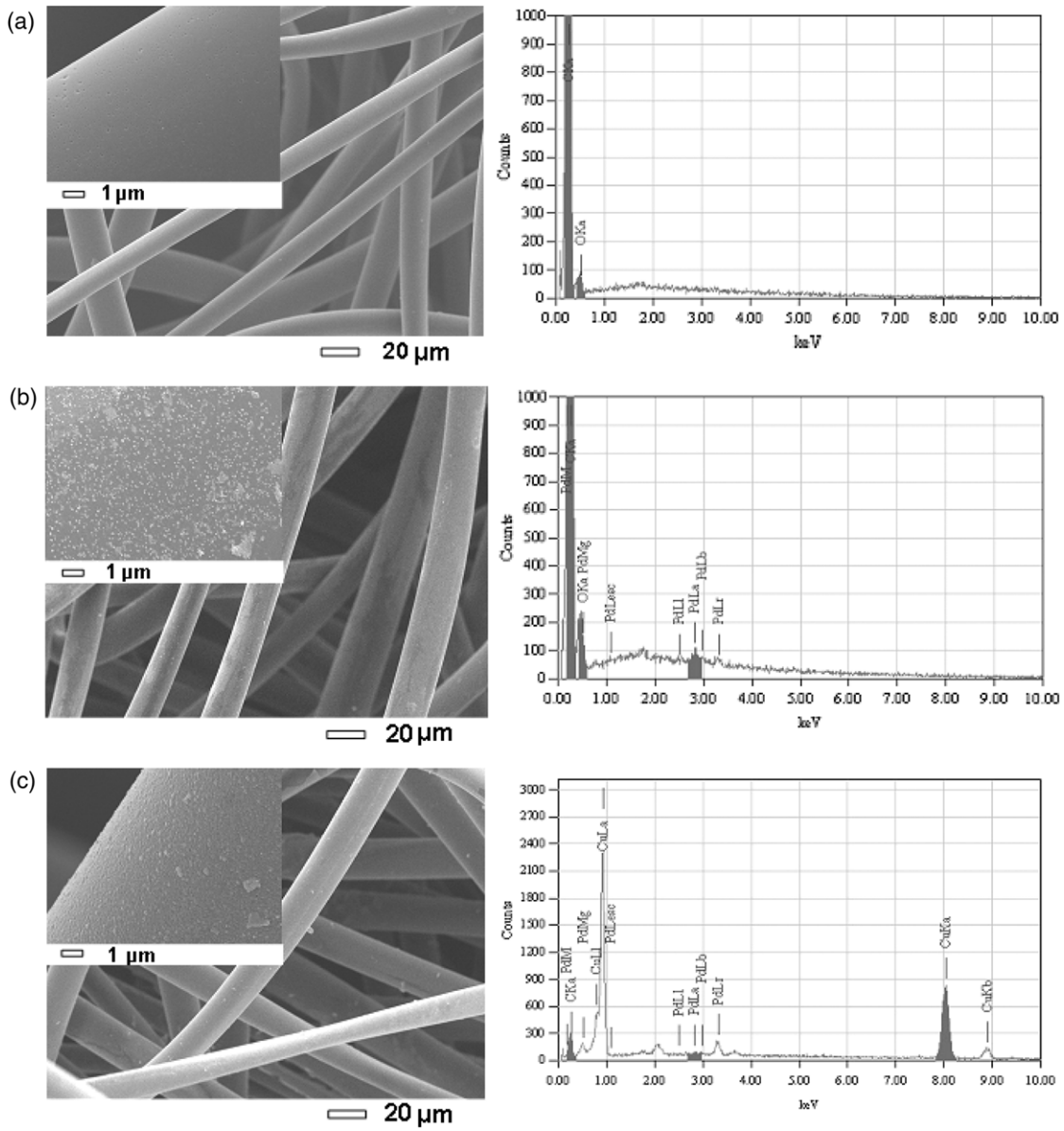

Figure 2. Morphological and chemical results of (*a*) pristine, (*b*) palladium activated and (*c*) copper deposited ACF.

in a copper ELD solution for the deposition of copper onto the surfaces of the activated ACF. The ACF was vigorously rinsed with deionized (DI) water after ELD to remove the residual solution and then dried. Two solutions were mixed and used for the ELD solution. Solution A contained 3 g of $CuSO_4$, 14 g of sodium potassium tartrate (Rochelle salt) and 4 g of NaOH in 100 ml of deionized water. Solution B was an aqueous formaldehyde solution (37.2 wt%). Solutions A and B were mixed at a 10 : 1 (v/v) ratio and the activated ACF was immersed into the mixture so that the copper particles would be coated on the activated sites.

Copper oxide was grown on the ACF surface by heating the copper deposited ACF in a furnace to the predetermined temperature (100, 300, 500 °C) for 1 h. NO/N_2 gas (1000 ppm NO) was delivered to the furnace at room temperature in order to prevent burn-off of the ACF. An absolute filter was used to filter any particulate contamination in the gas. The gas flow rate through the furnace was maintained at 1 L min^{-1} using a mass flow controller (MKS Instrument, US). The wall temperature of the furnace was increased from 100 to 500 °C [34, 35] using a proportional integral derivative (PID) temperature controller. A stainless steel (SS) mesh with a graphite gasket was used to support the ACF and minimize channelling.

Table 1. Chemical composition (qualified from ×50 000 specific SEM micrograph).

	Mass (%)			
Sample	C	O	Pd	Cu
Pristine	97.2	2.8	—	—
Palladium activated	97.9	1.0	1.1	—
Copper deposited	33.4	0.7	0.5	65.4
100 °C treated	55.0	3.6	0.2	41.2
300 °C treated	52.8	8.2	0.7	38.3
500 °C treated	49.6	14.2	2.1	34.1

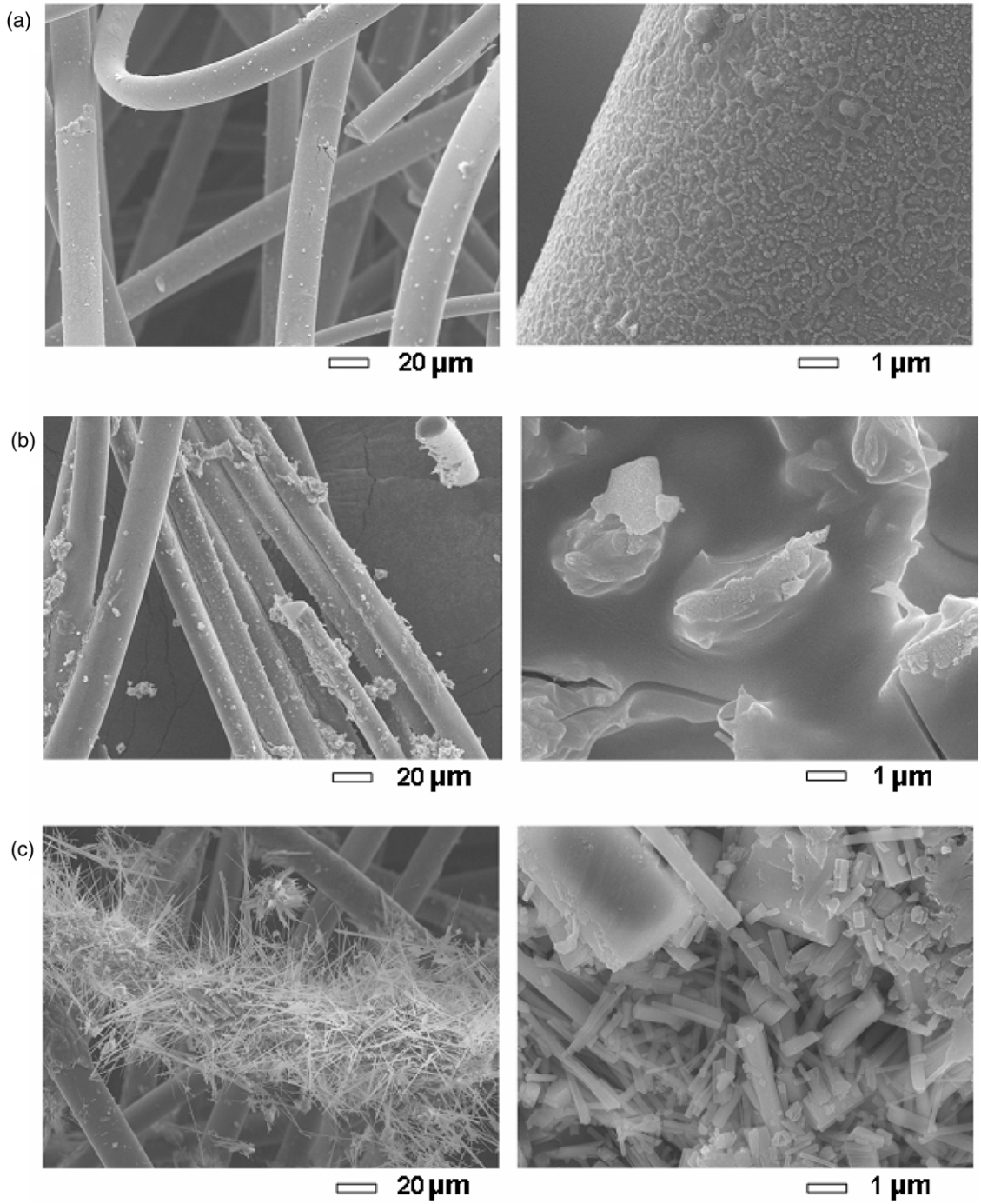

Figure 3. Morphology of samples at (*a*) 100 °C, (*b*) 300 °C and (*c*) 500 °C treated ACF.

The surface morphology of the ACF as well as the distribution of palladium, copper and copper oxide particles were examined by FESEM (JSM-6500F, JEOL, Japan). The chemical composition was determined by EDX (JED-2300, JEOL, Japan). The crystalline phases of the particles deposited on the ACF were examined by wide-angle XRD on a Rigaku Model D/MAX-Rint 2000 (Japan) diffraction meter using Cu Kα radiation ($\lambda = 0.154\,18$ nm) at 30 kV and 20 mA. A thin powder sample of the ACF was placed onto an oriented monocrystalline quartz plate and scanned from 10° to 100° (2θ) at 4° min^{-1}. The nitrogen adsorption isotherms of the ACF sample were measured using a porosimeter (ASAP 2010, Micromeritics Instrument Corp., US) at −196 °C with relative pressures ranging from 10^{-6} to 1. High purity (99.9999%) nitrogen gas was used as the adsorbent. All samples were degassed at 50 °C for 2 h before each measurement. The specific surface area was determined using the BET equation. The total pore volume, which was estimated based on the N_2 volume adsorbed at a relative saturation pressure (∼0.996), corresponded to the total amount adsorbed. The pore size distribution was determined using the Barrett, Joyner and Halenda (BJH) method, which uses the area of the pore walls

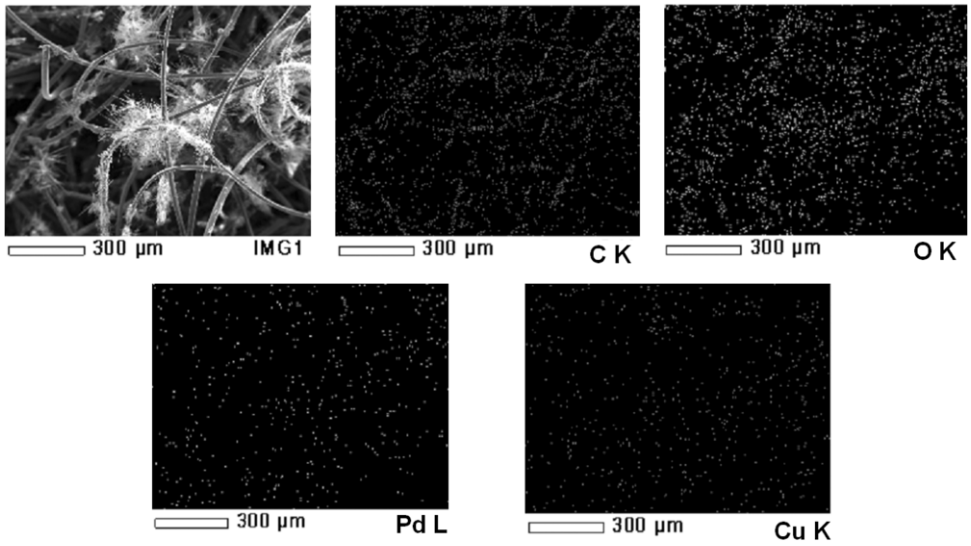

Figure 4. EDX map of 500 °C treated ACF.

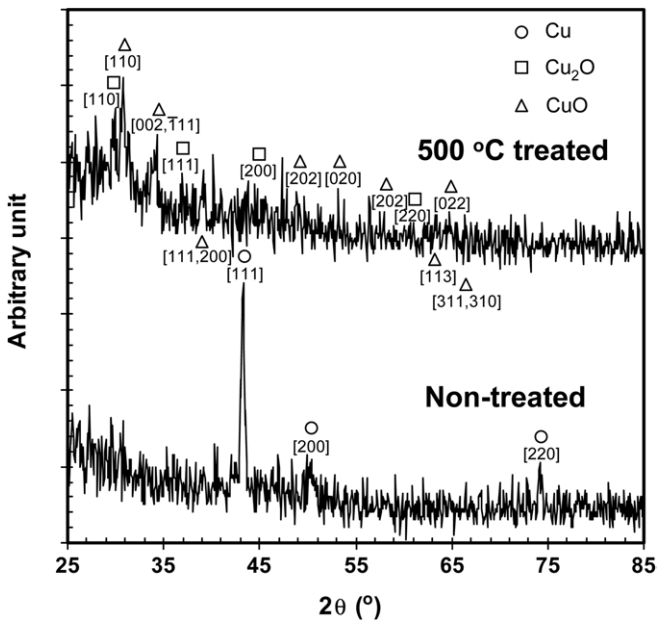

Figure 5. XRD patterns of copper deposited and 500 °C treated ACF.

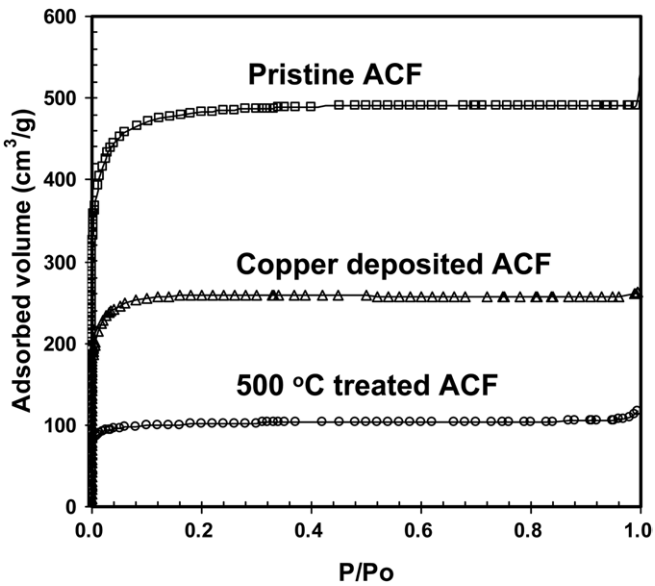

Figure 6. Adsorption isotherms of pristine, copper deposited and 500 °C treated ACF.

and the Kelvin equation to correlate the relative N_2 pressure at equilibrium with the amount of porous solid.

3. Results and discussion

Figures 2(*a*) and (*b*) show SEM micrographs of the pristine and palladium activated ACF, respectively. While the pristine ACF had a clean surface, a number of particles (about 30 nm in diameter) were observed on the activated ACF. EDX results (also shown in figures 2(*a*) and (*b*)) showed a small amount of palladium in the activated ACF but not on the pristine ACF. Figure 2(*c*) shows that after ELD, the ACF was coated uniformly and densely with sphere-shaped particles, approximately 25 nm in diameter. From EDX analysis (also shown in figure 2(*c*)), it was found that these particles were mainly composed of copper. Carbon and oxygen, which might have originated from the ACF, were also detected. Table 1 shows the chemical compositions of the pristine, palladium activated and copper deposited ACF.

Figure 3 shows SEM micrographs of the thermally treated ACF at operating temperatures from 100 to 500 °C. The colour of the copper deposited ACF was changed from brown to grey with the heat treatment. The surface morphology of the copper deposited ACF shown in figure 2(*c*) was slightly changed after the 100 °C treatment (figure 3(*a*)). The copper particles became larger as a result of coalescence between copper particles while relatively large uncoated areas were observed between the particle layers. At 300 °C (figure 3(*b*)), further coalescence of the particles occurred and the particles became sprout shaped. The treatment at 500 °C (figure 3(*c*)) produced remarkable changes in the microstructure of the

Table 2. Textural properties.

Sample	TSSA[a]	MSSA[b]	TPV[c]	MPV[d]	APD[e]
Pristine	1610 ± 48	1593 ± 51	0.87 ± 0.08	0.85 ± 0.08	17.7 ± 0.2
Copper deposited	1039 ± 33	1036 ± 21	0.41 ± 0.05	0.40 ± 0.02	17.2 ± 0.3
100 °C treated	1019 ± 41	1006 ± 33	0.40 ± 0.02	0.39 ± 0.03	16.9 ± 0.1
300 °C treated	869 ± 12	846 ± 21	0.37 ± 0.01	0.36 ± 0.03	16.6 ± 0.2
500 °C treated	401 ± 16	389 ± 14	0.18 ± 0.03	0.16 ± 0.01	16.1 ± 0.2

[a] Total specific surface area ($m^2\ g^{-1}$).
[b] Micropore specific surface area ($m^2\ g^{-1}$).
[c] Total pore volume ($cm^3\ g^{-1}$).
[d] Micropore volume ($cm^3\ g^{-1}$).
[e] Average pore diameter (Å).

particles. Stem-shaped particles grew on the ACF and a large number of stems, approximately 2 μm in width and 80 μm in length, were observed. This volumetric growth of copper particles has been reported by other investigators [2, 23, 35].

The first image in figure 4 shows a different scaled SEM micrograph of the 500 °C treated ACF. The other four images show the EDX maps of the first image. These maps correspond to carbon, oxygen, palladium and copper, respectively. The dots in these images indicate the positions of each element in the first image. For example, oxygen is concentrated in the regions corresponding to the copper particles in the first image, which shows that the particles contain a large amount of oxygen. Table 1 shows the chemical compositions of the 100, 300 and 500 °C treated ACF. The atomic oxygen concentration in the sample increased with increasing temperature but the copper concentration decreased.

Figure 5 shows XRD patterns of the non-treated and the 500 °C treated ACF. The XRD pattern of the non-treated ACF shows three peaks at 43.3°, 50.4° and 74.1° of 2θ. The data from the Powder Diffraction File No 04-0836 show that these peaks correspond to the (1 1 1), (2 0 0) and (2 2 0) planes of the face-centred cubic (fcc) phase for copper, respectively. The XRD profile for the non-treated ACF shows the characteristics of pure metallic copper with good crystallinity and without any impurity phases. The XRD pattern of the 500 °C is noisy. However, instead of copper, the pattern shows copper oxides, such as Cu_2O and CuO, which were referenced to the Powder Diffraction Files No 05-0667 and No 05-0661, respectively. The presence of the pattern noise indicates that the impurity may exist as an amorphous component because of a thermal energy, critical for crystallization of amorphous components [36]. The morphological evolution shown in figure 3 can be explained by the oxidation of copper.

During the heat treatment in a NO/N_2 gas flow, the copper on the ACF reacted with NO to produce N_2 and O_2. In this reaction, the copper was first converted to Cu_2O, which was transformed to CuO with further oxidation [24].

$$NO + Cu/ACF \rightarrow Cu_2O/ACF + 1/2N_2, \quad (1)$$

$$NO + Cu_2O/ACF \rightarrow CuO/ACF + 1/2N_2. \quad (2)$$

The oxygen produced was reduced to O^- and O_2^-, which were then diffused into the surface layer or interface [37]. Copper was oxidized to Cu^{2+} or Cu^+ to form Cu_2O and CuO [23]. In summary, copper played the role as a reductant in the reaction, as revealed by XRD.

To investigate the effect of copper deposition and heat treatment on the change in porosity of ACFs, textural properties of the copper deposited and heat treated ACFs were measured. Figure 6 shows that the largest uptake occurred at a relatively low pressure ($P/P_o < 0.1$) and reached a plateau at $P/P_o \approx 0.3$. This suggests that all ACF samples had microporous characteristics (type I isotherm) according to the IUPAC classification [38]. The adsorbed volume was the largest for the pristine ACF but decreased for the copper deposited and 500 °C treated ACF because the deposited copper particles and oxidized copper particles could obstruct or reside in some pores of the corresponding ACF support. Table 2 shows the textural properties of the samples. When copper deposition was performed, the specific area (from 1610 to 1039 $m^2\ g^{-1}$), pore volume (0.87–0.41 $cm^3\ g^{-1}$) and pore diameter (17.7–17.2 Å) decreased. As the temperature increased from 100 to 500 °C, the surface area and pore volume of the ACF decreased from 1019 $m^2\ g^{-1}$ to 401 $m^2\ g^{-1}$ and from 0.40 $cm^3\ g^{-1}$ to 0.18 $cm^3\ g^{-1}$, respectively. The further decrease in porosity was attributed to volume expansion [23] of copper particles during oxidation.

4. Conclusions

In this study, a novel method for fabricating Cu oxide/ACF through the aerosol Pd activation for use in electroless Cu deposition and heat treatment with NO gas injection. Cu ELD was initiated by catalytically activating the ACF surface with aerosol Pd nanoparticles. The catalytically activated ACF was placed into the solution for the ELD of Cu. When the Cu deposited ACF was subjected to a heat treatment in a NO/N_2 gas flow (1000 ppm NO), morphological changes to the Cu particles were observed due to volume expansion of the Cu particles during the treatment. As the temperature increased from 100 to 500 °C, the relative mass fraction of oxygen increased from 3.6% to 14.2% but the fraction of Cu decreased from 41.2% to 34.1% due to the formation of Cu oxides (Cu_2O and CuO). The corresponding surface area and pore volume of the ACF decreased from 1019 $m^2\ g^{-1}$ to 401 $m^2\ g^{-1}$ and from 0.40 $cm^3\ g^{-1}$ to 0.18 $cm^3\ g^{-1}$, respectively.

Acknowledgment

This study was supported by Seoul R&DB Program (Grant No 10593).

References

[1] Kumar R V, Elgamiel R, Diamant Y and Gedanken A 2001 *Langmuir* **17** 1406
[2] Zhang K, Rossi C, Tenailleau C, Alphonse P and Chane-Ching J-Y 2007 *Nanotechnology* **18** 275607
[3] Lee D W, Ha G H and Kim B K 2001 *Scr. Mater.* **44** 2137
[4] Das D and Chakravorty D 2001 *J. Mater. Res.* **16** 1047
[5] Marbán G, Antuña R and Fuertes A B 2003 *Appl. Catal.* B **41** 323
[6] Nickolov R, Stankova N, Khristova M and Mehandjiev D 2003 *J. Colloid Interface Sci.* **265** 121
[7] Wang Z *et al* 2008 *J. Colloid Interface Sci.* **320** 520
[8] Ozawa M, Suzuki S, Loong C-K, Richardson J W Jr and Thomas R R 1997 *Appl. Surf. Sci.* **121–122** 441
[9] Lee J K, Choi J, Kang S J, Lee J M, Tak Y and Lee J 2007 *Electrochim. Acta* **52** 2272
[10] Deng C, Shi P F and Zhang S 2006 *Electrochim. Acta* **51** 5349
[11] Papadimitropoulos G, Vourdas N, Vamvakas V E and Davazoglou D 2005 *J. Phys. Conf. Ser.* **10** 182
[12] Ogwu A A, Bouquerel E, Ademosu O, Moh S, Crossau E and Placido F 2005 *Acta Mater.* **53** 5151
[13] Hwang Y, Park H S, Lee J K and Jung W H 2006 *Curr. Appl. Phys.* **6** e67
[14] Borkow G, Sidwell R W, Smee D F, Barnard D L, Morrey J D, Lara-Villegas H H, Shemer-Avni Y and Gabbay J 2007 *Antimicrob. Agents Chemother.* **51** 2605
[15] Yang C M and Kaneko K 2002 *J. Colloid Interface Sci.* **246** 34
[16] Moon J S, Park K K, Kim J H and Seo G 2000 *Appl. Catal.* A **201** 81
[17] Chen S and Zeng H 2003 *Carbon* **41** 1265
[18] Matatov-Meytal Y and Sheintuch M 2002 *Appl. Catal.* A **231** 1
[19] Park S J and Kim B J 2005 *J. Colloid Interface Sci.* **282** 124
[20] Tanahashi I 2005 *Electrochem. Solid-State Lett.* **8** A627
[21] Ko T-H, Hung K-H, Tzeng S-S, Shen J-W and Hung C-H 2007 *Phys. Scr.* **T129** 80
[22] Nakagawa H, Shudo A and Miura K 2000 *J. Electrochem. Soc.* **147** 38
[23] Kim I S and Lee S K 2005 *Scr. Mater.* **52** 1045
[24] Park S J and Kim B J 2005 *J. Colloid Interface Sci.* **292** 493
[25] Chujiang C, Xiaozheng Y, Zhigang S and Yushan X 2007 *J. Phys. D: Appl. Phys.* **40** 6026
[26] Kim G G, Kang J A, Kim J H, Lee K-Y, Kim S J and Kim S-J 2007 *Scr. Mater.* **56** 349
[27] Pascu M, Debarnot D, Poncin-Epaillard F, Bumbu G G, Cimmino S and Vasile C 2006 *J. Phys. D: Appl. Phys.* **39** 2224
[28] Touchais-Papet E, Charbonnier M and Romand M 1999 *Appl. Surf. Sci.* **138–139** 557
[29] Byeon J H, Yoon H S, Yoon K Y, Ryu S K and Hwang J 2008 *Surf. Coat. Technol.* **202** 3571
[30] Borra J-P 2006 *J. Phys. D: Appl. Phys.* **39** R19
[31] Byeon J H, Ko B J and Hwang J 2008 *J. Phys. Chem.* C **112** 3627
[32] Byeon J H, Yoon K Y, Jung Y K and Hwang J 2008 *Electrochem. Commun.* **10** 1272
[33] Byeon J H, Park J H and Hwang J 2008 *J. Aerosol Sci.* **39** 888
[34] Holzschuh H and Suhr H 1990 *Appl. Phys.* A **51** 486
[35] Saka M, Yamaya F and Tohmyoh H 2007 *Scr. Mater.* **56** 1031
[36] Bastide S, Duphil D, Borra J-P and Lévy-Clément C 2006 *Adv. Mater.* **18** 106
[37] Rhead G E 1965 *Trans. Faraday Soc.* **61** 797
[38] Brunauer S, Emmett P H and Teller E 1938 *J. Am. Chem. Soc.* **60** 309